www.sciencemag.org/cgi/content/full/329/5994/967/DC1

Supporting Online Material for

Cell Lineage Reconstruction of Early Zebrafish Embryos Using Label-Free Nonlinear Microscopy

Nicolas Olivier, Miguel A. Luengo-Oroz, Louise Duloquin, Emmanuel Faure, Thierry Savy, Israël Veilleux, Xavier Solinas, Delphine Débarre, Paul Bourgine, Andres Santos, Nadine Peyriéras,* Emmanuel Beaurepaire*

*To whom correspondence should be addressed.
E-mail: nadine.peyrieras@inaf.cnrs-gif.fr (N.P.),
emmanuel.beaurepaire@polytechnique.edu (E.B.)

Published 20 August 2010, *Science* **329**, 967 (2010)
DOI: 10.1126/science.1189428

This PDF file includes:

Other Supporting Online Material for this manuscript includes the following:
(available at www.sciencemag.org/cgi/content/full/329/5994/967/DC1)

Supplementary Materials

Materials and Methods

Supplementary Figures

Supplementary Movies

References

1. D. Oron, E. Tal, Y. Silberberg, *Opt Lett* **28**, 2315 (Dec 1, 2003).
2. J. P. Levraud *et al.*, *J Immunol* **178**, 4385 (Apr 1, 2007).
3. C. B. Kimmel, W. W. Ballard, S. R. Kimmel, B. Ullmann, T. F. Schilling, *Dev Dyn* **203**, 253 (Jul, 1995).
4. D. Débarre *et al.*, *Nat. Methods* **3**, 47 (2006).
5. D. Débarre *et al.*, *Opt. Lett.* **29**, 2881 (2004).
6. M. A. Luengo-Oroz *et al.*, in *5th IEEE International Symposium on Biomedical Imaging: From Nano to Macro (ISBI)*. (Paris, 2008), pp. 504-507.
7. C. Vachier, F. Meyer, *Journal of Mathematical Imaging and Vision* **22**, 251 (2005).
8. J. Fernandez, M. Valladares, R. Fuentes, A. Ubilla, *Dev Dyn* **235**, 656 (Mar, 2006).
9. P. J. Keller, A. D. Schmidt, J. Wittbrodt, E. H. Stelzer, *Science* **322**, 1065 (Nov 14, 2008).

Materials and Methods

Microscopy

Imaging was performed with a custom-built laser scanning 2PEF-SHG-THG microscope equipped with detection channels in the backward (epi) and forward (trans) directions. Excitation was performed using an optical parametric oscillator (OPO) (APE, Germany) synchronously pumped by a titanium:sapphire oscillator (Coherent Inc., USA). The OPO provided an 80MHz train of 100-150fs pulses with 1.1-1.2µm center wavelength at the focus of the objective. The microscope incorporated galvanometer-mounted mirrors (GSI Lumonics), Z-motorized water-immersion objectives (20× 0.95 numerical aperture (NA) and 60× 1.2 NA, Olympus, Japan), photon-counting photomultiplier modules (ET Enterprises Ltd., UK), lab-designed counting electronics, and filters (695CDXRU Chroma Technology Corp, USA; 390/40, 600/14, Di510 Semrock, USA). Scanning and signal acquisition were synchronized using LabView software and a multichannel I/O board (National Instruments, USA).
Simultaneous THG/SHG imaging was performed with trans-detection of both signals. A half-wave plate was inserted in front of the scanners to control the incident polarization. SHG and THG signals were co-optimized by using rotating linear incident polarization, since THG and SHG efficiency have contradictory requirements in terms of incident polarization. SHG from mitotic spindles is reduced with incident linear polarization orthogonal to the spindle axis. Circularly polarized light is thus required to get similar signal levels from all spindles parallel to the imaging plane. However THG with circular incident polarization vanishes in isotropic media (*1*) and THG imaging should be performed using linear polarization. For 3-color imaging, simultaneous 2PEF imaging of mCherry fluorescence (Figure 2) was performed in epidetection. Large-scale images were recorded using the 20× objective with its pupil under-filled (resulting in 0.75 effective NA) providing 3.5 µm axial (and sub-µm lateral) resolution in THG images. High-resolution images were recorded using a 1.2 NA 60× (water immersion) objective resulting in 1.2 µm axial resolution in THG images at the embryo surface. Power after the objective was typically 200 mW with 1200 nm excitation, and was adjusted with imaging depth (see conformal scanning). Pixel rate was ~300kHz.
Raw data visualization was performed with ImageJ (NIH, USA) and Amira (Visage Imaging Inc. USA). Image processing was performed with a dedicated algorithmic workflow described below. Data analysis was performed with Matlab (Matworks). Interactive visualization and annotation of reconstructed and raw data (augmented phenomenology) was performed with our custom built interface Mov-IT (written in Java).

Fish strains

Embryos were obtained from natural spawning of wild type or transgenic fish lines. Transgenic fish *ßactin:H2B/mcherry* (*2*) were used for the maternal expression of mCherry fusion protein with nuclear localization.

Embryo mounting

mCherry membrane staining was obtained through 1 cell stage injection of 200 pg *mcherry-ras* synthetic mRNA (mMessage mMachine kit, Ambion). Injected embryos were raised at 28.5°C for the next 3 hours. Embryos were mechanically dechorionated and mounted in a microchamber consisting of a Teflon tore with a 780 µm diameter hole inserted into a 5 mm hole at the bottom of a 3cm Petri Dish sealed with a coverslip. Embryo was maintained within the hole of the Teflon tore and properly oriented by infiltrating 0.5% low melting point agarose (Sigma) in embryo medium. For animal pole view imaging, agarose was kept below the blastoderm margin to avoid biomechanical constraints. Temperature control in the room resulted in a temperature of about 22±1°C under the objective, and development was slowed down compared to the standard 28.5°C developmental table (*3*). After imaging, embryo morphology was checked under the dissecting binocular and the animal was raised for at least 24h to assess morphological defects. Imaged embryos could be raised to adulthood and were fertile.

Conformal acquisition settings

Conformal scanning was performed by scanning the focal point along spiral trajectories with variable galvanometer speed and illumination intensity, in successive planes separated by 3µm or 4µm, throughout a half sphere (440 µm radius) encompassing the entire blastoderm and YSL. Variable scanning speed was implemented as follows: the galvanometer command voltages targeted an Archimedes spiral with a constant radial step and a linear variation of sampling density along the trajectory, while the pixel clock was kept constant. The innermost blastoderm region was oversampled and innermost yolk regions were under-sampled in order to optimize the imaging speed. The sampling density was roughly kept constant at the surface of the embryo, and the laser power was adjusted for each plane. See figure S1. Samples were then projected into a Cartesian XY grid, taking into account the sampling density.

Assessing light-induced perturbation

Harmonic microscopy with >1.1µm excitation wavelength and illumination rates similar to those used here have been described as preserving physiological conditions (*4, 5*) The reduced two-photon absorption by endogenous cell structures at these wavelengths explains this relative harmlessness. However, illumination should be controlled and we developed a specific methodology to assess light-induced perturbation.
(i) Comparison of different illumination rates
First, we showed that the spatio-temporal distribution of the division pseudo-waves observed using three different imaging conditions with different illumination rates were similar (less than 10% variability): “fast” conformal scanning ($2\times2\times4\mu m^3$, 110 planes, 80s/stack), “slow” conformal scanning ($1.5\times1.5\times3\mu m^3$, 150 planes, 3min/stack), and raster scanning (that did not reveal mitosis in tissue depth); $1.5\times1.5\times3\mu m^3$, 140 planes, 5min/stack.
(ii) THG signature of local perturbation.
We defined a criterion for “safe” illumination conditions by using our observation that sustained illumination (150mW, 1.2µm, 0.8NA, 1 image every 5s during more than 3min) of a single plane caused an increase of cytoplasmic THG signal (Figure S2A-C). This perturbation appeared to depend on the imaging rate rather than on the total energy delivered to the

sample. This cytoplasmic THG signal did not correlate with immediate cell death or block embryo development, and progressively disappeared in the absence of further illumination. This perturbation was observed only in the illuminated planes, suggesting a nonlinear process of multiphoton absorption rather than linear absorption (e.g. by water).

(iii) Chosen imaging conditions

in toto time lapse imaging was performed with a time step of 80s at most, scanning speed at the periphery of the embryo was increased (×1.5) and excitation intensity was decreased (÷2). Such conditions were at least 5× less intensive than the ones used in Figure S2D and that did not trigger THG-positive cellular perturbation.

Image processing pipeline

SHG/THG image processing was performed using a specifically designed pipeline. SHG peak at metaphase was used to detect mitosis, while THG images were used to extract cell shape. The processing pipeline is outlined in Figure S4. Data from both SHG and THG channels (steps 1, 2) were filtered to remove experimental noise (steps 3,4). SHG 3D stacks corresponding to a given cycle were automatically binned into one frame (step 5). Sequences typically consisting of one hundred time points were reduced to ten frames, each corresponding to a division cycle. In parallel, segmentation of the outermost cell layer of the embryo was extracted from THG data by means of mathematical morphology operators (step 6). SHG data from step 5 and the embryo external surface (THG) were used to extract the lineage tree. Finding the two intensity maxima corresponding to mitosis at cell stage 2 initialized the procedure. A Voronoi partition was generated inside the embryo mask from the positions of the detected nuclei, providing a first robust approximation of membrane shape (*6*). Finding two symmetric SHG maxima in the next division cycle inside the Voronoi region assigned to their mother allowed identifying daughter cells (step 7). The number of SHG spots (2, 4, 8, etc.) corresponding to the current cell cycle were automatically detected, and corresponding mitoses were manually validated and corrected with the Mov-IT interface (step 8). Then, the Voronoi partition was generated from the detected spots inside the embryo mask of the next cell cycle and the procedure of automatic detection and validation/correction was iterated for the successive division cycles (steps 7-8). The complete workflow allowed to extract all the cell centers and their lineage. However, mitosis temporal coordinates were not accurately defined at this stage. The timing information was extracted for each division from SHG intensity maxima along the temporal dimension using Gaussian fitting of the original data. We also took into account the acquisition delay between the first slice of the 3D stack and the current image (one image stack typically consisted of 110-150 images, acquired in 80s). Finally, the lineage tree was expanded to its original time length (step 9). Cell nuclei positions were further used for seeding a more precise cell contours detection based on a viscous watershed segmentation algorithm (*7*) applied to THG images (step 10). Measurements obtained through this image processing workflow were saved in a database (Oracle) and interactively used with the Mov-IT interface. Methods were implemented in Matlab and processing a time lapse encompassing the first 10 cell cycles took 72h of computation time on a Core2duo platform with 8 GB RAM, and 4h of user interaction for manual checking of the detected SHG spots and script launching.

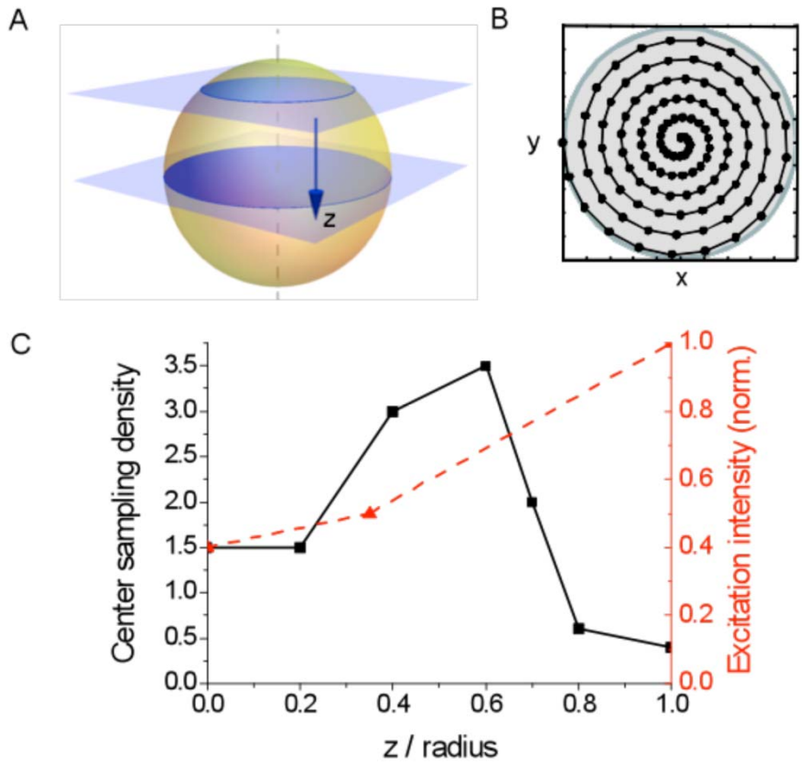

Figure S1: Conformal acquisition settings

A: Schematized spherical zebrafish embryo imaged from the animal pole and z sectioning of a half sphere containing blastoderm and YSL. B: Each plane was scanned along a spiral trajectory with variable sampling density and constant pixel clock (corresponding to variable scanning speed). C: Sampling density at the center of the spiral (plain black curve, squares) and relative excitation intensity (dashed red curve, triangles) as a function of the imaging plane z normalized to the sphere radius.

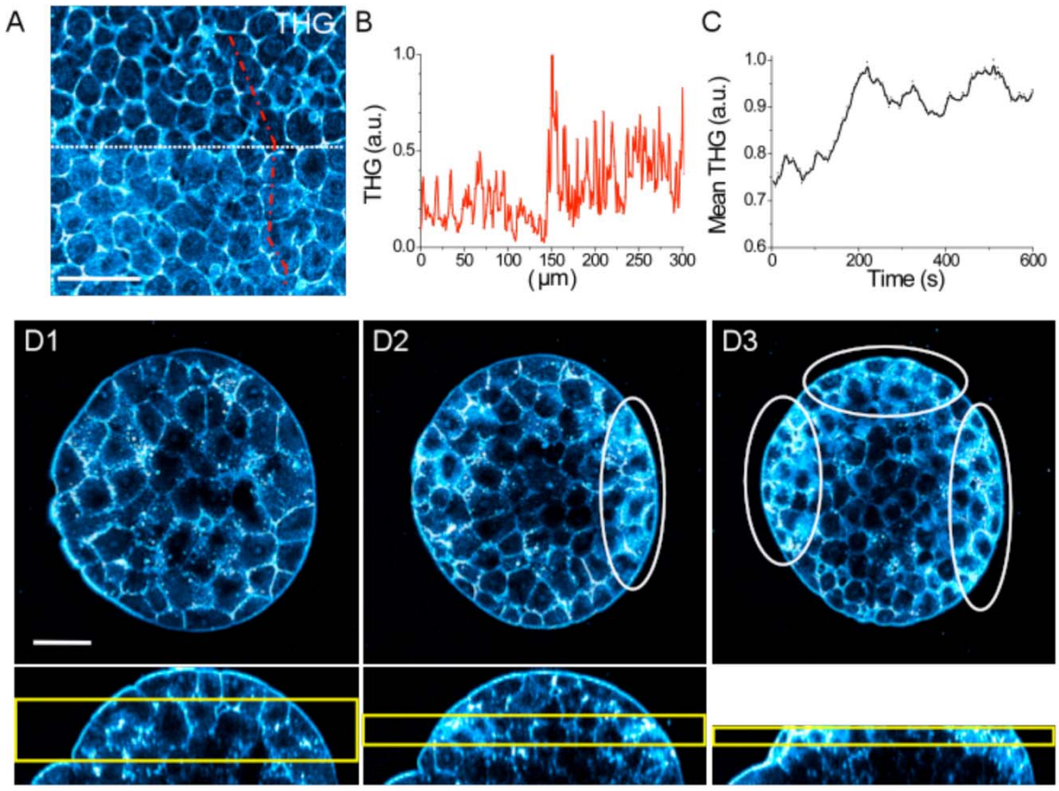

Figure S2: Onset of phototoxicity probed with cytoplasmic THG signal

A-D: a developing embryo was imaged continuously through early cleavage stages during successive periods of 12 minutes using raster scanning with different imaging rates. Single planes were recorded every 1.2s and separated axially by 3µm. The following imaging parameters were used: 1.2 µm wavelength, 100 fs pulses after the objective, 0.8NA, 150 mW average power, 1.5×1.5×3 μm^3 voxels, 370 µm/ms scanning speed, 2.2 ms/line.
A: THG section in the blastoderm at cell stage 128 after sustained illumination of the area below the white dotted line: 150 mW, 1.2 µm, 0.8NA, 1 image every 5s during 12min. B: Spatial profile of the THG signal across the red dashed line in (A), average signal from the cytoplasm is ~twice higher in the illuminated region. C: Temporal evolution of the average THG signal in the illuminated region, showing a rapid increase after ~3min. D1-3: THG images of an embryo submitted to different local illumination rates but with total illumination kept constant; the thickness of the illuminated region was changed from 100 µm (D1) to 50 µm (D2) and 25 µm (D3), meaning that a given plane was illuminated every ~40s (D1), 20s (D2) and 10s (D3); top panels are XY planes, bottom panels are XZ projections; yellow rectangles indicate the previously illuminated volume. Scale bars, 100 µm.
These experiments indicated that the tissue could locally tolerate illumination up to a certain rate, beyond which intracellular alterations became visible (see embryo periphery in D2-3) Therefore, distributing a given illumination dose over the entire embryo was less harmful than delivering it to a restricted volume.

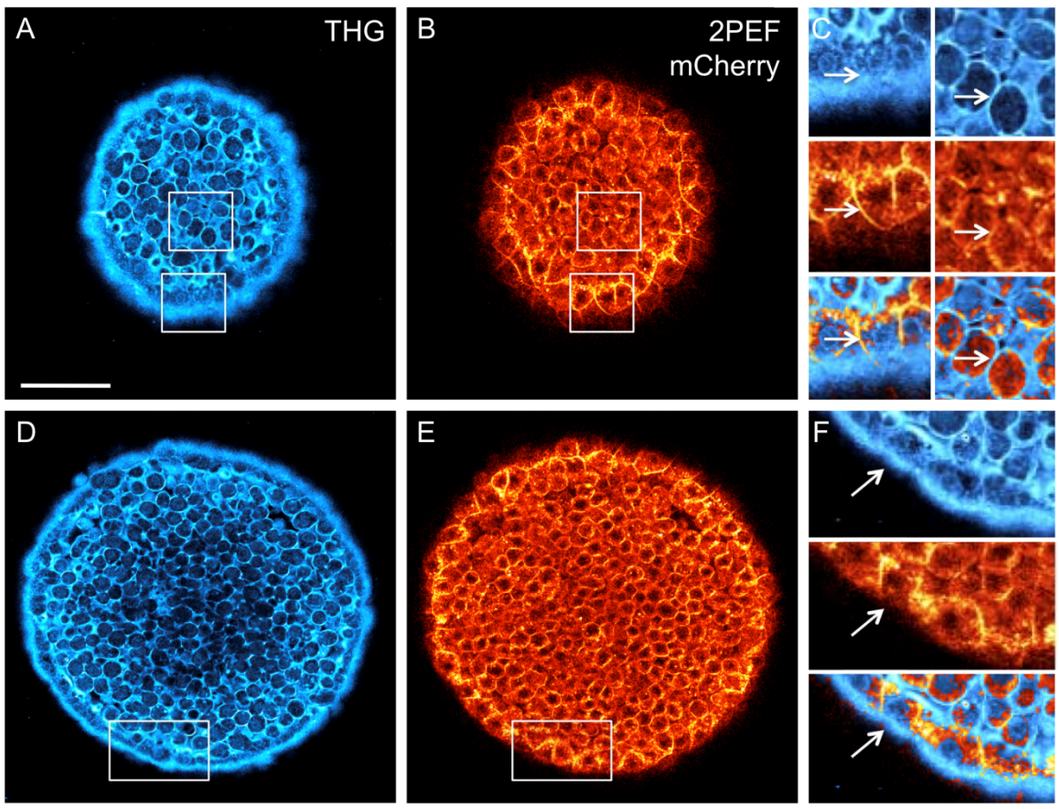

Figure S3: Comparison of THG and farnesylated mCherry signals

Combined THG/2PEF images were recorded at 2 different depths in a membrane-labeled embryo at stage High (*3*). Membrane staining by farnesylated mCherry was obtained through mRNA injection (see Materials and Methods). A,D: THG images. B,E: 2PEF revealing mCherry staining. Magnification (2.2×) of the white squares in (A) and (B) shown in C. Magnification (2,2×) of the white square in (D) and (E) shown in F. C: left panel shows the EVL with the white arrow pointing to lateral cell membrane; left panel deep cells with white arrow points to the cell membrane. Note that THG brightly highlighted the embryo surface but did not reveal EVL cells lateral contours. Conversely, farnesylated mCherry did not localize at the apical surface of the outer epithelium but stained baso-lateral membranes. Note that deep cell contours are better revealed by THG than by farnesylated mCherry. Scale bar: 100µm.

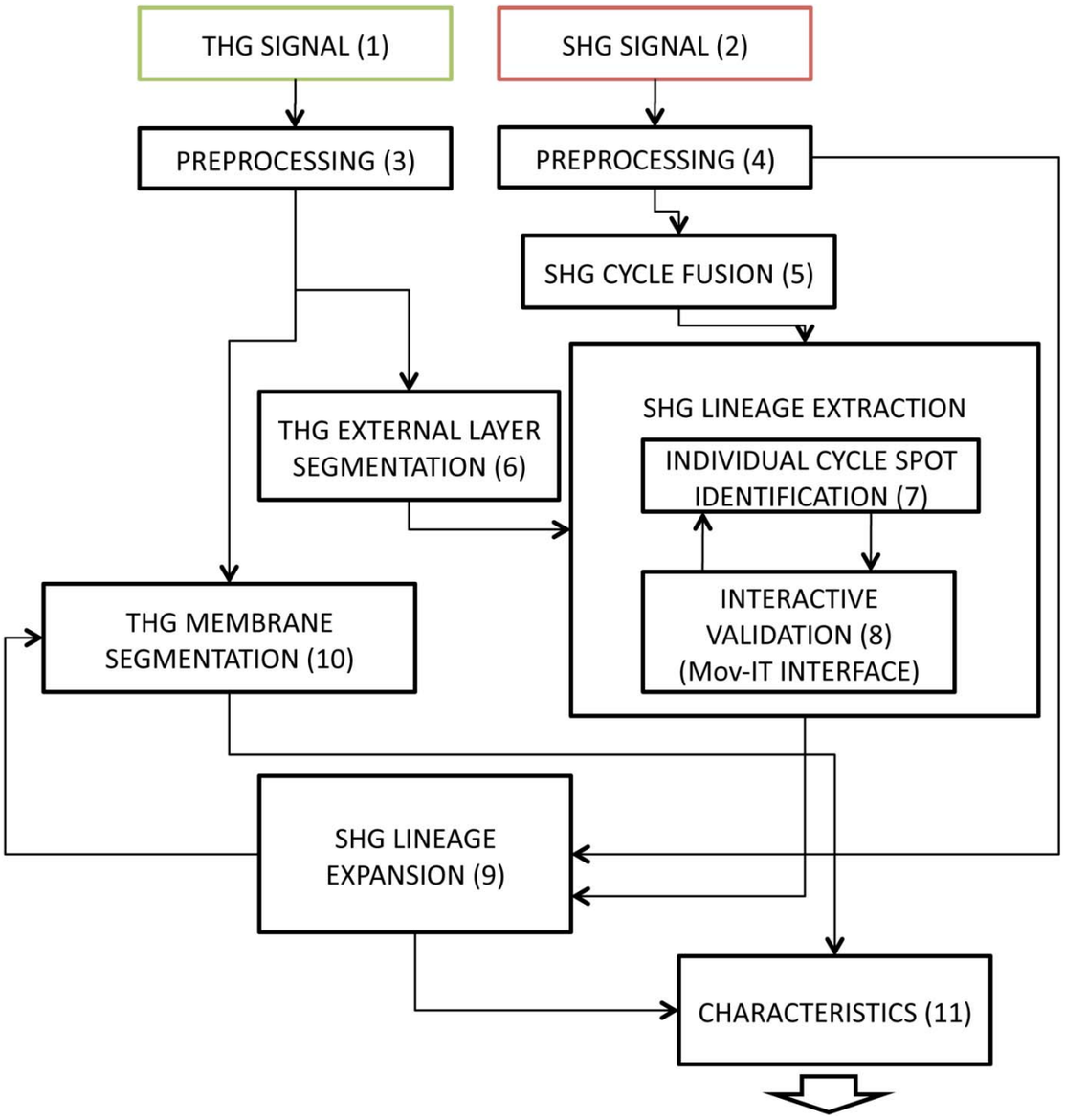

Figure S4: Algorithmic pipeline for processing THG/SHG data from cleavage stages

Schematic representation of the different steps described in Materials and Methods. Step 1 and Step 2: data from both SHG and THG channels; Step 3 and Step 4: filtering; Step 5: SHG stacks time binning; Step 6: segmentation of outer cell layer; Step 7: finding two symmetric SHG maxima for daughter cells inside the Voronoi region assigned to their mother; Step 8: SHG spots correction and validation for each cell cycle and generation of Voronoi partition from the detected spots inside the embryo mask of the next cell cycle; Step 9: Gaussian fitting to extract precise mitosis timing, expansion of the lineage tree to its original time length; Step 10: Cell nucleus position was further used for seeding a more precise cell contours detection based on a viscous watershed segmentation algorithm applied to THG images; Step 11: Measurements obtained through this image processing workflow were saved in a database (Oracle) and interactively used with the Mov-IT interface.

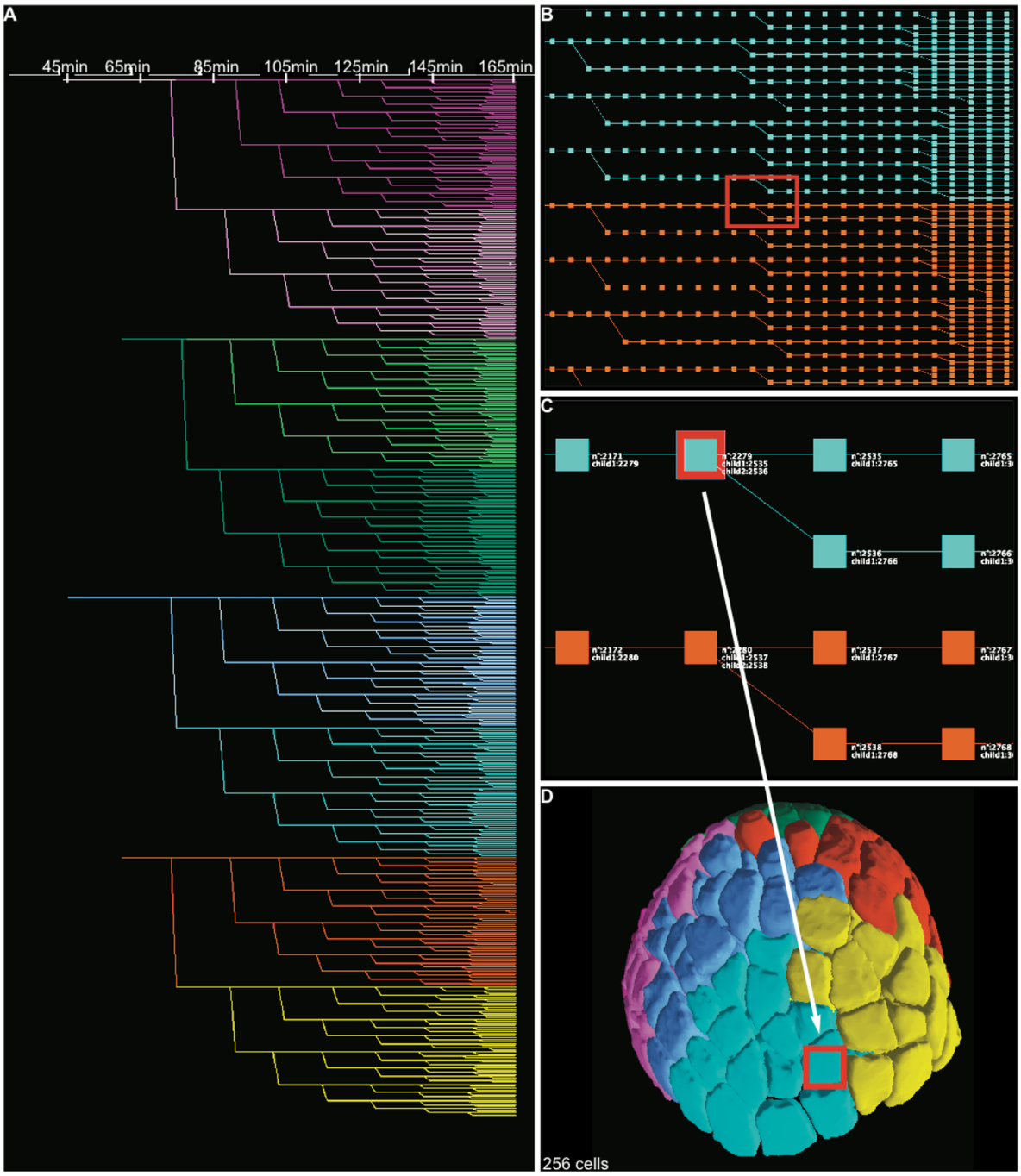

Figure S5: Visualization of the cell lineage tree

Custom-built visualization interface (Mov-IT) allowed to visualize the reconstructed lineage tree either with a flat representation or with a 3D rendering and superimposed raw data. See Movie M07. A: Lineage tree from 2 to 512 cells with binary branches indicating mitosis, timing indicated at the top from left to right, colors correspond to the clonal progeny of the first 8 blastomeres as in Figure 3F-J, red box magnified in B. B: magnification of the tree shown in A, each square corresponds to a cell at one time point, time step is 90 sec, red box magnified in C. C: magnification of the tree shown in B, each cell is annotated with its ID number, the cell highlighted with a red border is shown in (D). D: Volume rendering of the whole embryo at 256-cell stage, red square highlighting the same cell as in C.

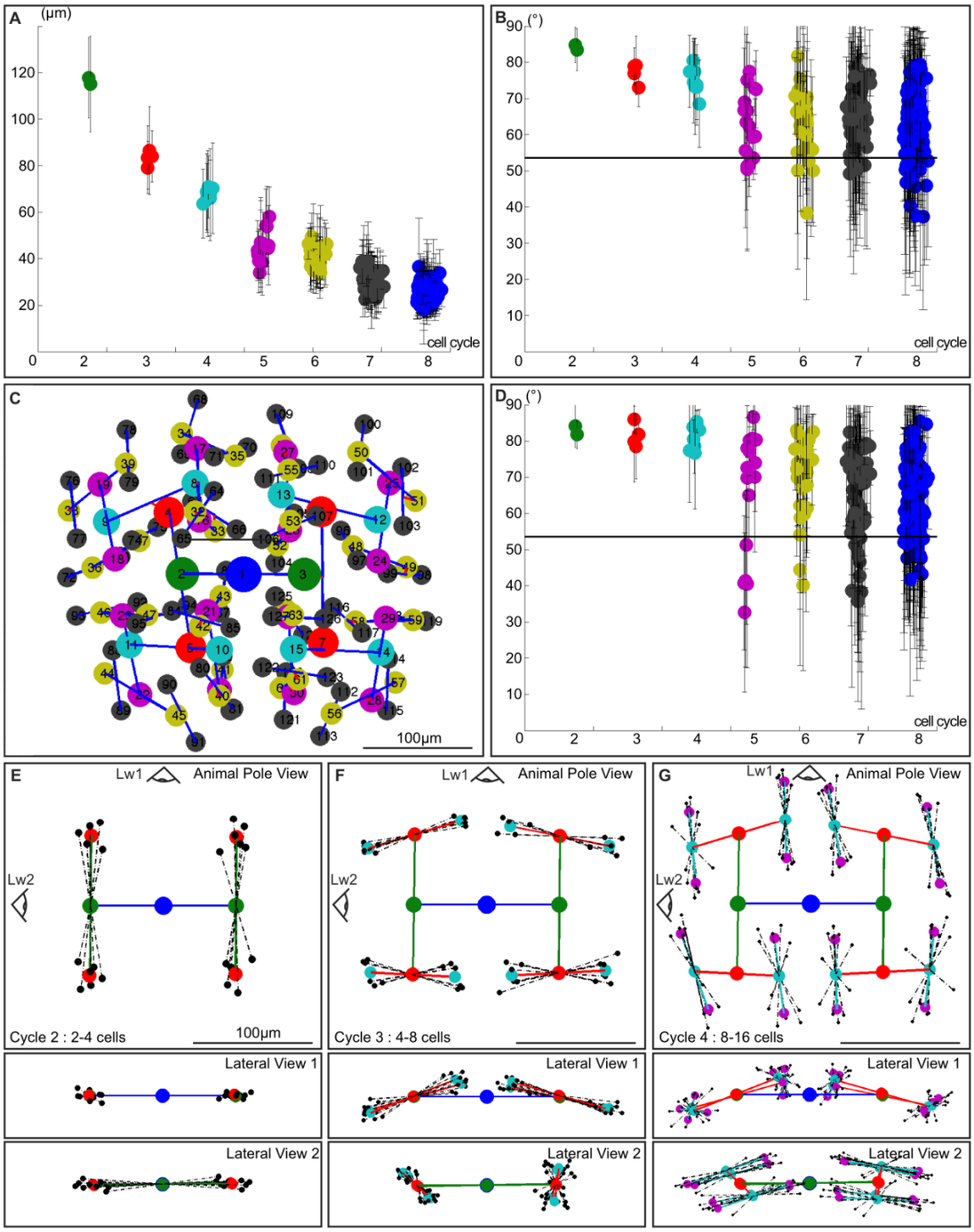
A
(µm)
cell cycle
B
(°)
cell cycle
C
100µm
D
(°)
cell cycle
E
Lw1
Animal Pole View
Lw2
Cycle 2 : 2-4 cells
100µm
F
Lw1
Animal Pole View
Lw2
Cycle 3 : 4-8 cells
G
Lw1
Animal Pole View
Lw2
Cycle 4 : 8-16 cells
Lateral View 1
Lateral View 2
Lateral View 1
Lateral View 2
Lateral View 1
Lateral View 2

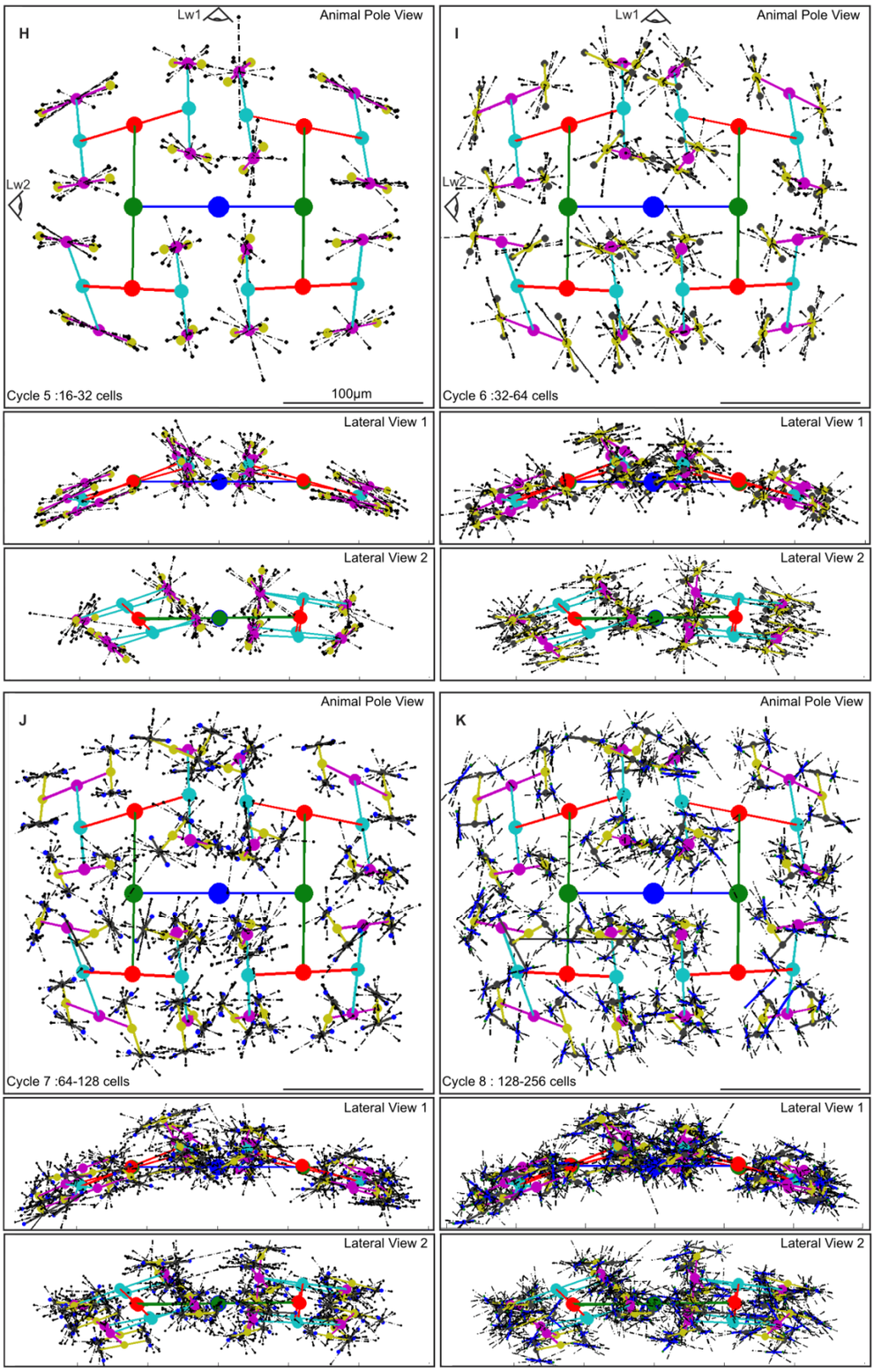

Figure S6: Division orientation and cell lineage spatial deployment

A: Distance between sister cells nuclei centers (i.e. “sister cells dipole” size) as a function of time. B: Angle between successive sister cells dipoles in degrees. Note that random orientation would provide an average of 55° indicated by the black line. C: Cells identification and schematized spatial deployment of divisions for one embryo. This was repeated for 6 different embryos and served as a basis for calculating a prototype. D: Angle between sister cells dipole and the normal to the embryo surface defined at the middle of the dipole. Cells divided tangentially to the embryo surface until cycle 5 (16-32). At cycle 5 (in purple), the 4 central blastomeres divided orthogonally to the embryo surface leading to a second cell layer (angle smaller than 55°). E-K: animal pole projection, prototypic representation showing the variation in daughter cells dipole orientation for each cell cycle (black dots and black dotted lines). Cell positions at previous stages were displayed in a prototypic embryo calculated from the six embryos of the cohort. From cycle 2 (in E) to cycle 8 (in K) fluctuation in the sister cells dipole orientation from one embryo to the other increases, although successive divisions keep displaying a privileged orientation orthogonal to the previous one.

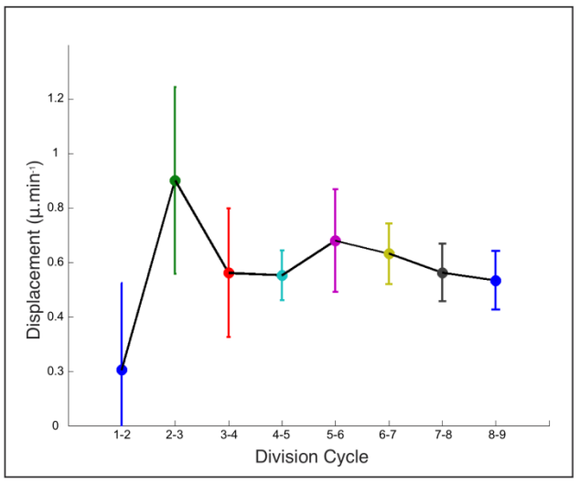

Figure S7: Cell displacements

Cell displacement speed was calculated for the 6 embryos of the cohort until cell cycle 10. Displacements were estimated as the distance between the position of a cell nucleus and the middle of the sister cells dipole after its division. The mean displacement for the 6 embryos is plotted a function of cell cycle. From cycle 3 to cycle 9, cell displacement stays in the range of 0.5 µm/min.

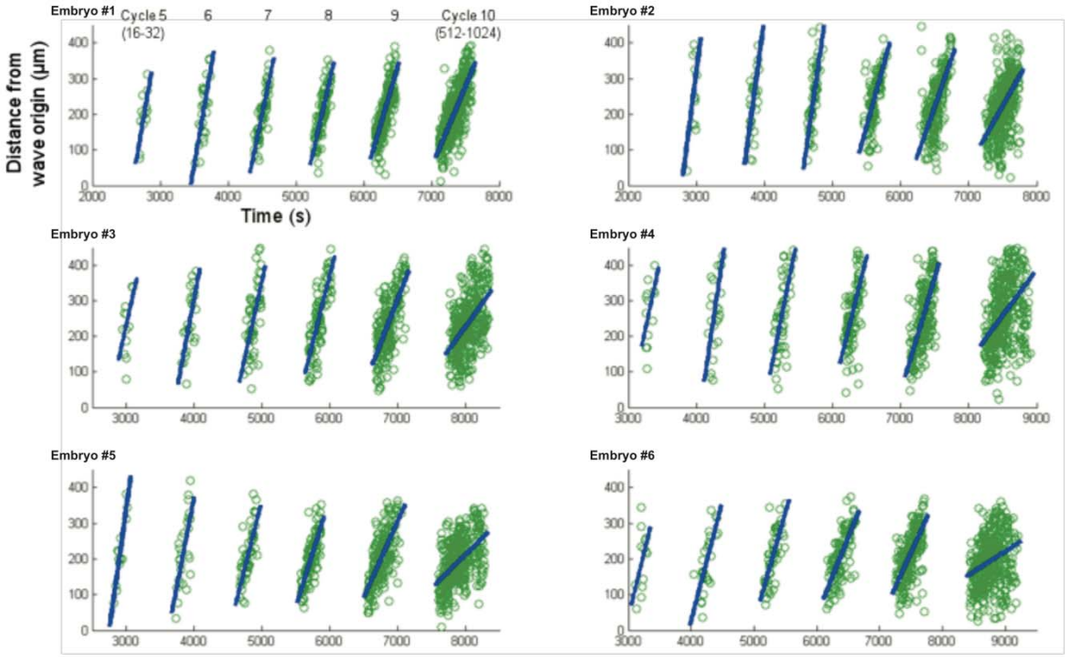

Figure S8: Mitotic pseudo-wave pattern during cycles 5-10 in six different embryos

Green circles are scatter plots of mitosis time (metaphase) as a function of distance to the pseudo-wave origin. Blue lines indicate the result of the linear fitting used to calculate pseudo-wave speed, and highlight mitoses spatio-temporal correlation. Note that dispersion around the linear fit increases with time.

	Cycle5	Cycle6	Cycle7	Cycle8	Cycle9	Cycle10
Embryo1	0.74	0.74	0.87	0.84	0.80	0.75
Embryo2	0.43	0.70	0.77	0.67	0.61	0.44
Embryo3	0.52	0.70	0.66	0.81	0.68	0.52
Embryo4	0.53	0.61	0.68	0.63	0.67	0.41
Embryo5	0.93	0.69	0.76	0.78	0.67	0.49
Embryo6	0.48	0.73	0.73	0.71	0.62	0.27
Mean	**0.61**	**0.70**	**0.74**	**0.74**	**0.68**	**0.48**

Table S9: Correlation coefficient (R) between division time and cell position during cycles 5-10

R values >0.5 indicate a strong spatio-temporal correlation between the cell cycle duration and the cell position relative to the pseudo-wave origin close to the animal pole. The corresponding p-values (probability of obtaining similar correlation coefficients in case of a random event) are $p<0.001$ in cycles 6-10 and $p<0.1$ in cycle 5. It should be noted that a marked decrease in this correlation happens at cycle 10 only and that a higher variability in R-value is observed at that stage.

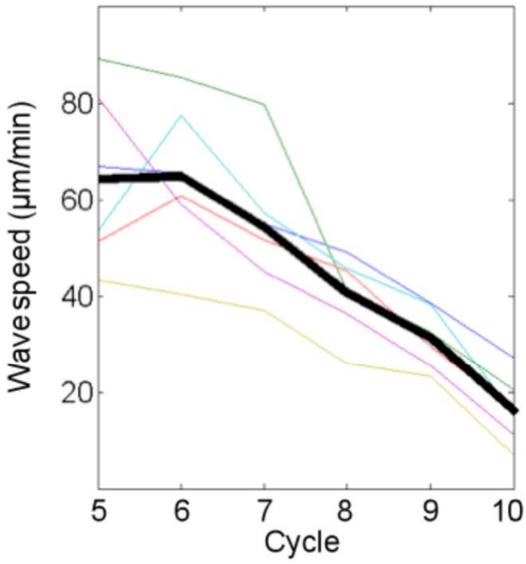

Cycle	5	6	7	8	9	10
Average wave speed (µm/min)	64.2	64.7	54.2	40.6	31.3	16.1
Standard deviation	18.1	15.7	14.5	8.4	6.4	7.1

Figure S10: Propagation speed of the division pseudo-waves

The speed of the mitotic pseudo-waves was estimated by linear fitting of the distance-to-pseudo-wave-center versus time. Pseudo-wave starting points were measured for each division cycle by calculating the weighted average of the first 5-10% mitoses. Top panel: plot of pseudo-wave speed versus division cycle for six embryos. The thick black line is the average. Bottom panel: mean and standard deviation of the estimated pseudo-wave speed.

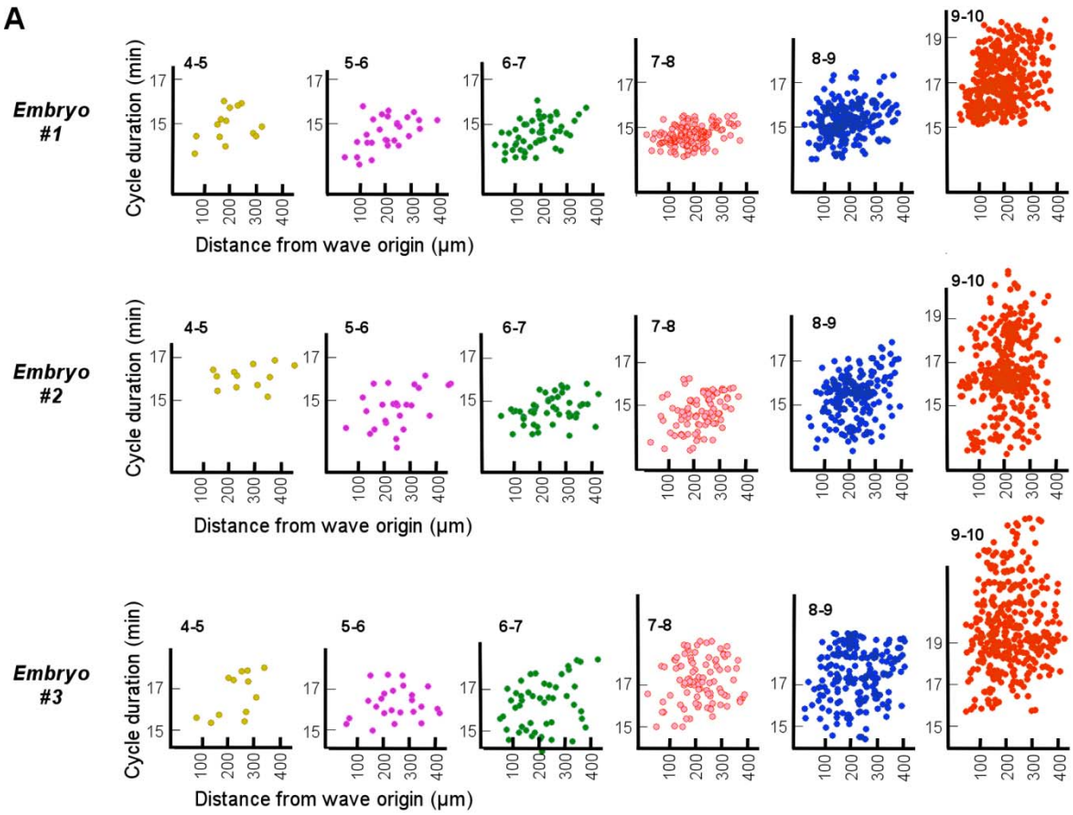

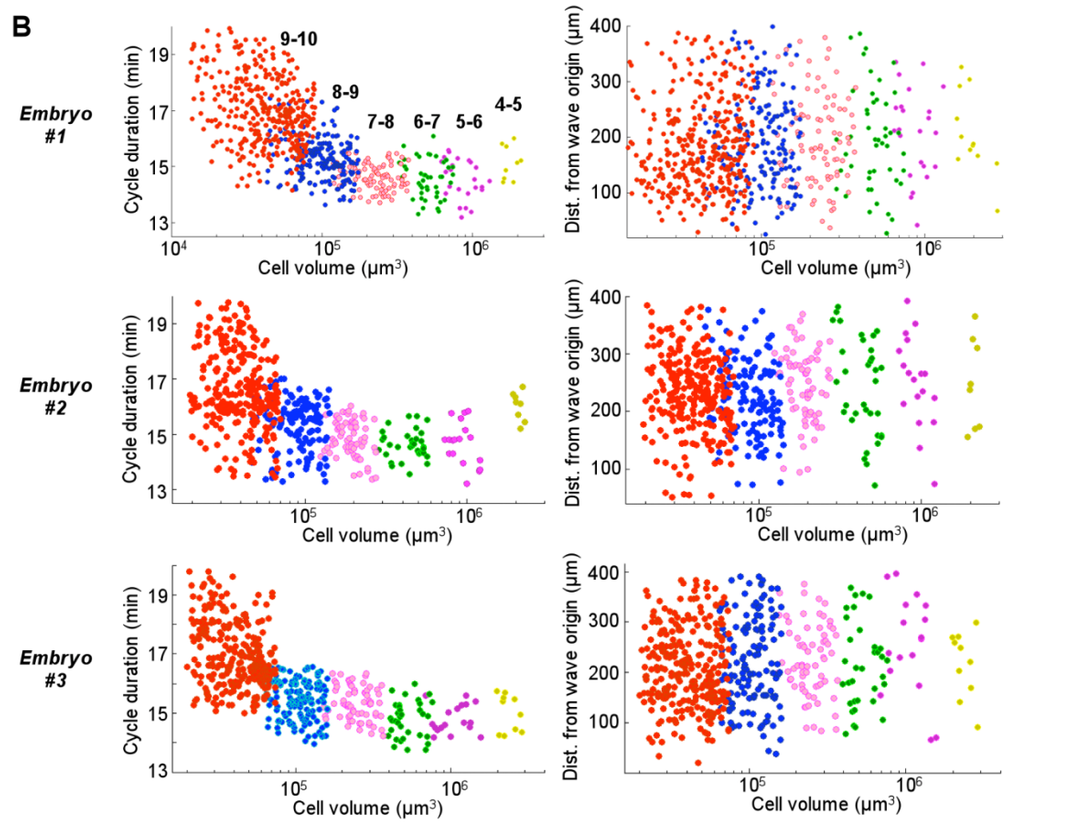

C

	Cycle5	Cycle6	Cycle7	Cycle8	Cycle9	Cycle10
C-D (N=6)	0,44	0,25	0,33	0,22	0,19	0,11
D-V (N=3)	-0,35	-0,38	-0,17	-0,12	-0,02	-0,03
C-V (N=3)	-0,47	-0,22	0,07	-0,14	-0,15	-0,24
T-D (N=6)	0.61	0.70	0.74	0.74	0.68	0.48

Figure S11: Pseudo-wave pattern characteristics analyzed in three different embryos

A: Cell cycle duration expressed as a function of distance from the pseudo-wave origin for individual cells during successive mitotic pseudo-waves, in 3 embryos. Although cell cycle duration exhibits variability, it correlates with the spatial position of the dividing cell. It should however be noted that increasing dispersion is observed, progressively breaking the pseudo-wave pattern.

B: Assessing a possible correlation of cycle duration or distance to pseudo-wave origin with cell volume in 3 embryos. B left: Cell cycle duration is expressed as a function of cell volume. B right: distance to pseudo-wave origin as a function of cell volume. Individual cell volume is increasingly variable through cell cycles and does not allow to predict cell cycle

duration. Cell volumes and spatial position exhibit limited correlation during cycles 5-7 (right column plots) as cells near the animal pole (pseudo-wave origin) are larger and divide faster.
C: Correlation coefficients (R) between cell cycle duration (C), distance to the pseudo-wave starting point (D), and cell volume (V). Correlation between distance D and division time T is given for comparison (from figure S8). For the calculation of correlation involving volume V, the largest and the smallest 10% of estimated values were omitted to avoid artifacts related to volume measurement errors. Similarly, for correlation calculations involving cycle duration C, the longest and shortest 10% of cycles were omitted to avoid outliers.

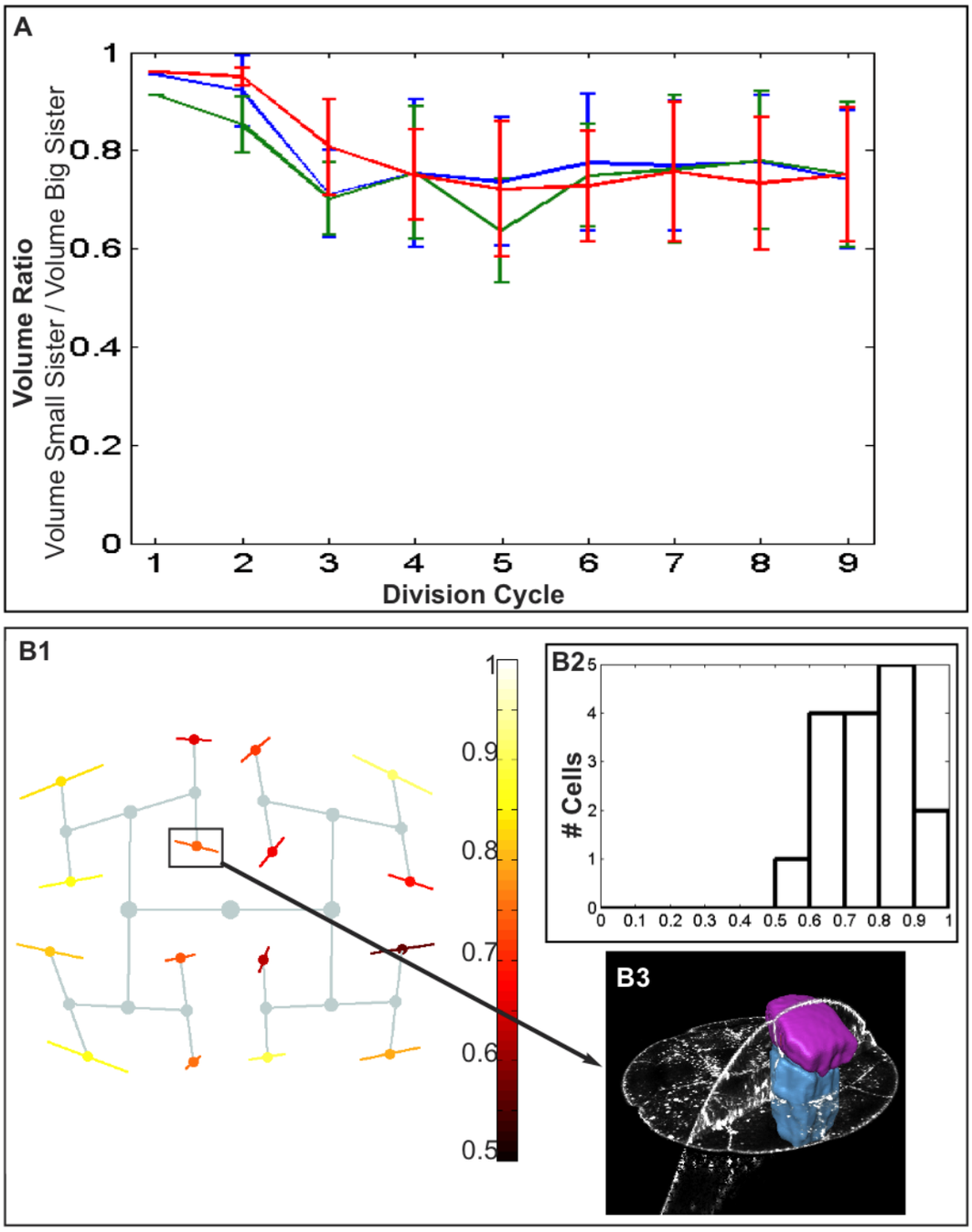

Figure S12: Sister cells' volume ratio

A: Sister cells' mean volume ratio expressed as the volume of the smaller sister divided by the volume of the larger one for three different embryos.

B: Spatial distribution of volume asymmetry at the 32-cell stage. B1: Sister cells dipoles have been colored according to the volume ratio. B2: Histogram of the number of sister cells from B1 with a given volume ratio. B3: Volume rendering of sister cells with a volume ratio of 0.75.

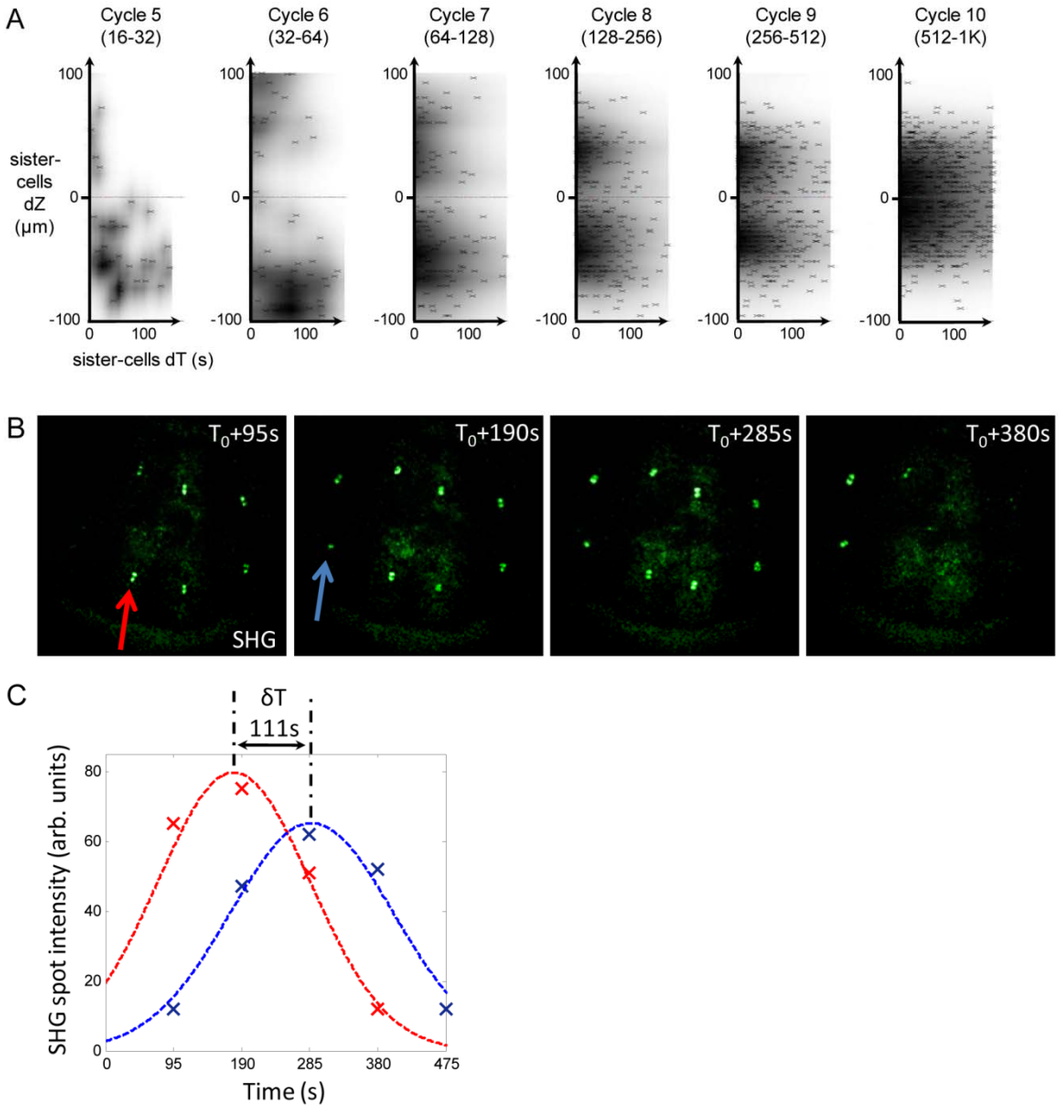

Figure S13: Division asymmetry

A: Plots of the relative position along the animal-vegetal axis (dZ) versus relative cell cycle length (dT) for sister cells, at each cell cycle (in one embryo). Our data reveals asymmetry (i.e. phenotypic difference between sister cells) at least during cycles 5-7: the “top” sister (i.e. the cell closest to the animal pole and to the pseudo-wave origin) exhibits a shorter cycle (i.e. time until next mitosis). B: SHG images show that asymmetric divisions happen at cycle 3. Red and blue arrows indicate sister cells that divide asynchronously at division 4 and display their SHG peak with approximately 2 minutes delay. C: Gaussian fits of the temporal evolution of the corresponding SHG signals providing measurement of the delay.

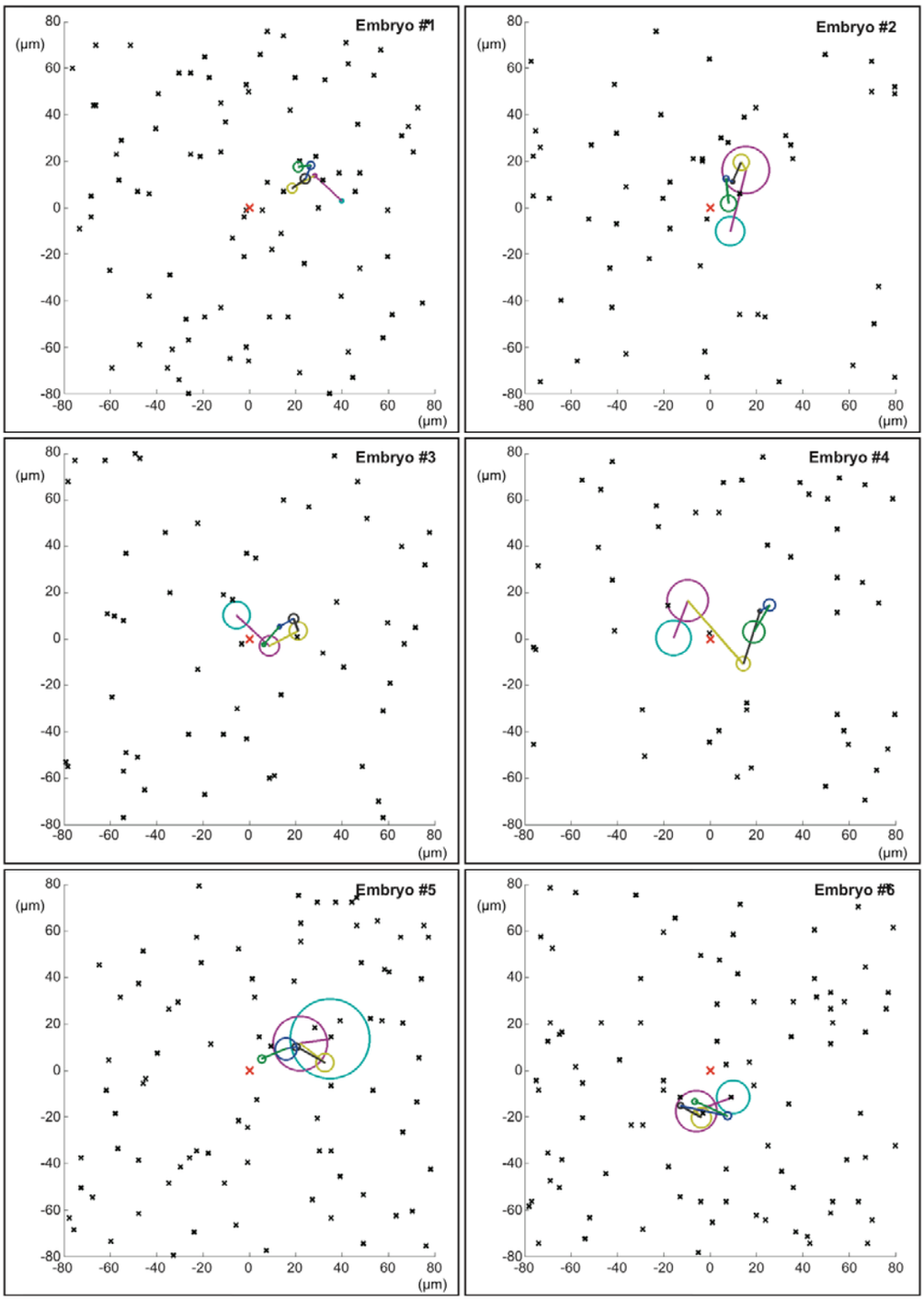

Figure S14: Mitotic pseudo-wave center in 6 different embryos

Same as Figure 5F, with six different embryos. Each embryo was defined by its ID number, indicated top right. Projection of the blastoderm with black crosses indicating the position of all the mitoses from cycle 10. The position of the pseudo-wave origin for cycles 5 to 10 (colored circle with its diameter indicating its variation during the pseudo-wave propagation) with respect to the animal pole (red cross) is displayed. Cycle 4 cyan, 5 purple, 6 yellow, 7 brown, 8 blue, 9 green.

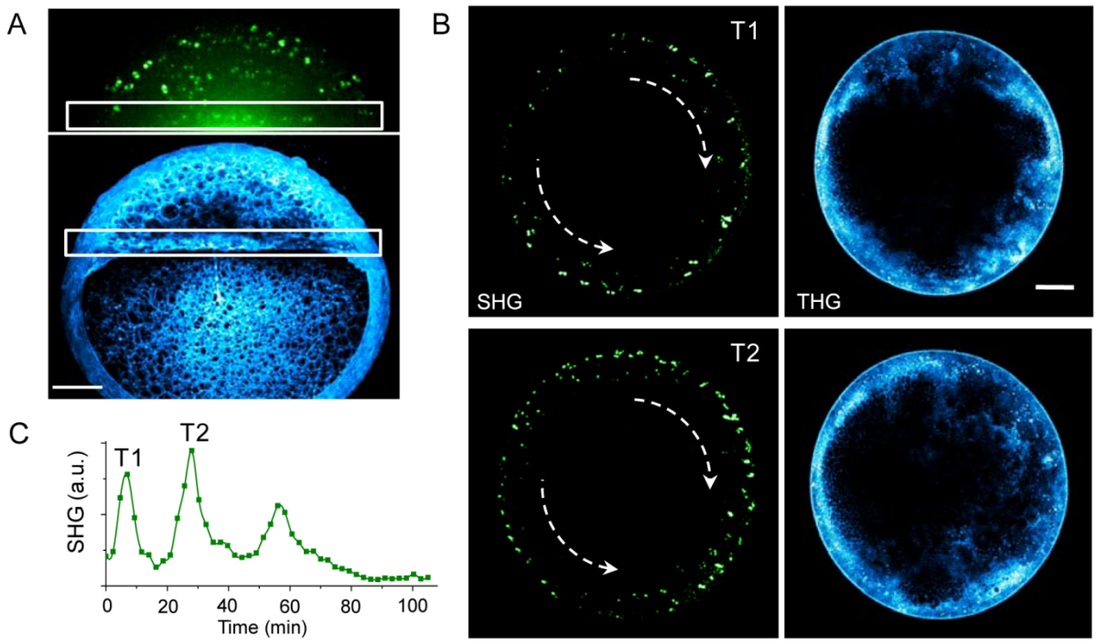

Figure S15: Distinct patterns for blastoderm and YSL division cycles

A: SHG (top panel) and THG (bottom panel) projections of z stacks encompassing the blastoderm margin at cell stage 1000, lateral view, animal pole to the top. White square indicates dividing YSL nuclei (see Movie M14).
B: SHG/THG imaging of the YSL division cycles from the animal pole. Left panels: SHG images show mitosis in the YSL with a peripheral pseudo-wave pattern, (see Movie M15); dotted arrows indicate the pseudo-wave propagation. Right panels: THG images confirm that divisions detected in the SHG channel happened in the YSL (no cell membranes). Two consecutive divisions are shown: T1 in upper panels, T2 in bottom panels. C: Time evolution of the SHG signal during YSL mitoses indicated that in this data set, yolk nuclei underwent three divisions.

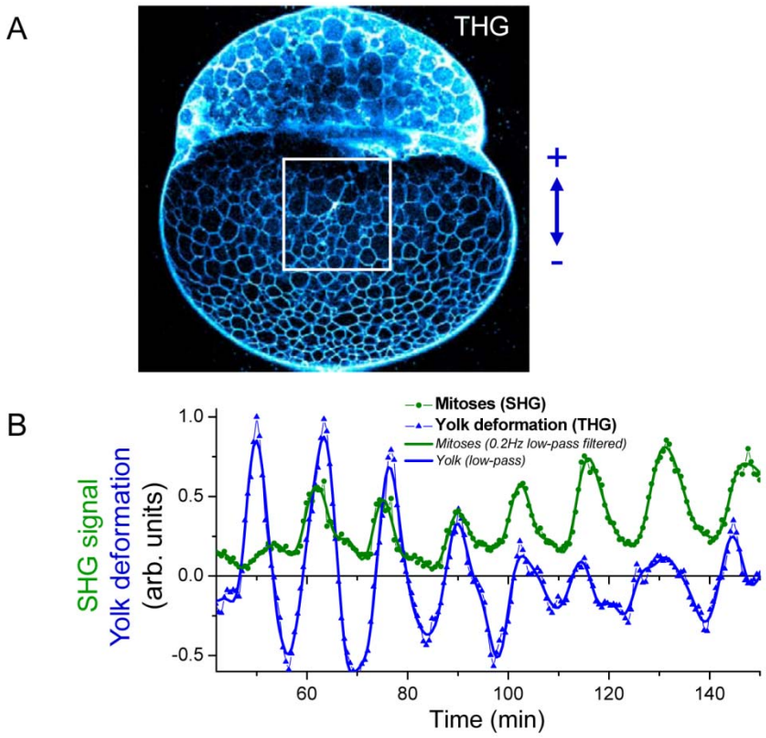

Figure S16: Mitotic pseudo-waves and yolk deformations

A: 80-100 µm thick sagittal slice of the zebrafish embryo was imaged for THG with 30s temporal resolution (see Movie M01). Post fertilization, yolk streams drive cytoplasm to the animal pole. Thereafter, the yolk displays foam-like arrangement of platelets (*8*). Yolk deformations seem to correlate with blastoderm division cycles. White square indicates the region where measurements are made (see movie M01).
B: Oscillation of yolk platelet position was measured using 2D correlation analysis in each plane, and results were averaged over the entire slice. Yolk deformations (blue) are synchronized with mitotic cycles in green (SHG signal), and dampen after 64-cell stage.

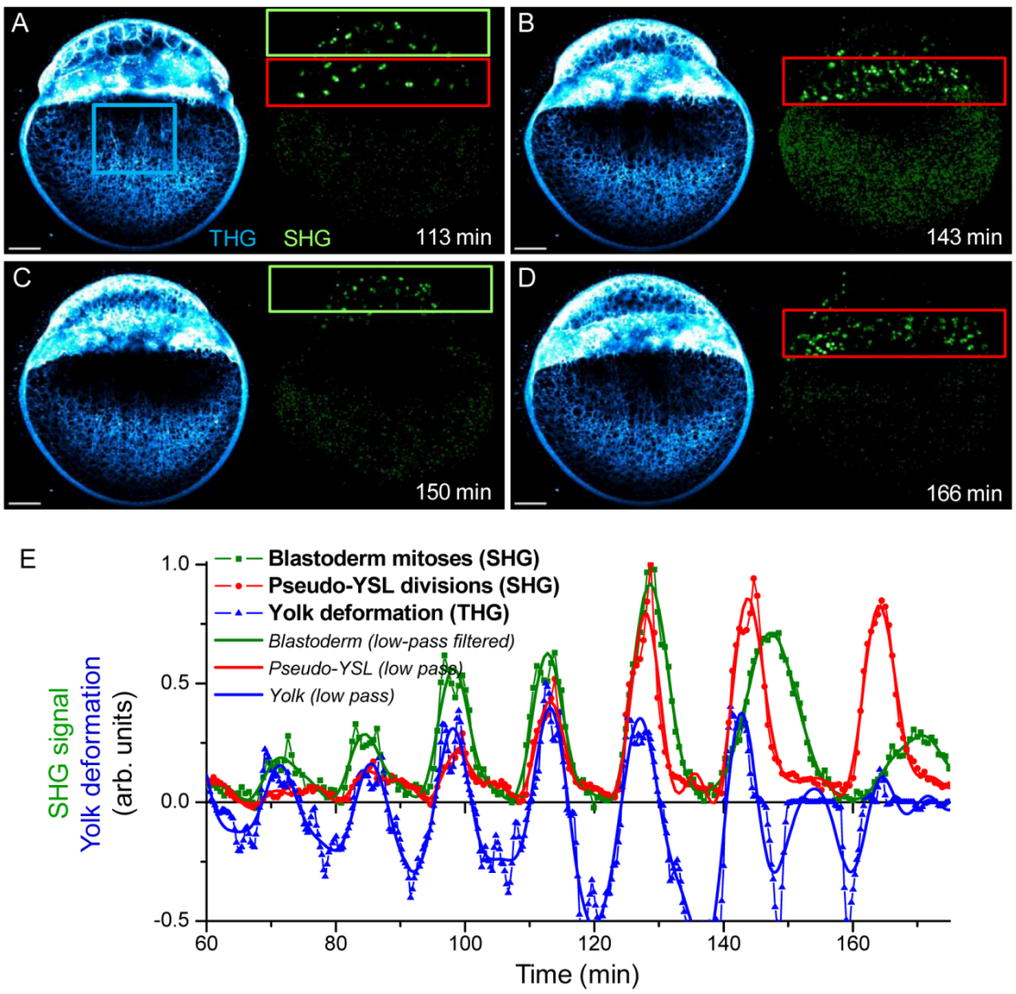

Figure S17: Artifact in YSL formation under biomechanical constraint

A-D: THG-SHG time lapse imaging, one cell stage embryo embedded in 1% low melting point agarose (Sigma) and showing at an early stage a large YSL (red box) with a division pattern distinct from the blastoderm (green box) (See Movie M16). These mounting conditions were similar to those used for SPIM/DSLM imaging (*9*) and led to the appearance of early YSL peripheral pseudo-waves. THG signal is in blue, SHG in green. 4 different time points are displayed (indicated bottom right). Scale bar 100 µm. E: deformations along the animal-vegetal axis (THG in blue), nuclear divisions in the enlarged YSL (SHG intensity in red measured in the red box in A-D) and mitoses in the overlying blastoderm (SHG intensity in green measured in the green box in A-D) as a function of time. YSL division pseudo-waves remained synchronized with periodic yolk deformations.

Supplementary Movies

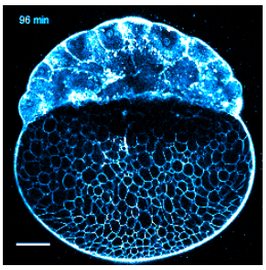

Movie M01: THG imaging of the zebrafish embryo from the one-cell stage

Time-lapse, THG imaging from the one-cell stage as in figure 2A. A sagittal thick slice is displayed. Excitation wavelength: 1200nm. Excitation NA ~0.75 (20× objective). Scale bar: 100µm. Imaging time indicated top left. Raw data visualized with ImageJ software.

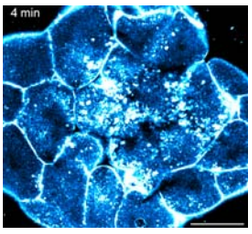

Movie M02: Membrane dynamics and vesicular trafficking at the yolk blastoderm interface

THG image, magnification of a single section in the depth of the blastoderm from 32-cell stage to 64-cell stage. THG highlights membrane completion at the yolk blastoderm interface. Scale bar: 100µm. Raw data visualized with ImageJ software.

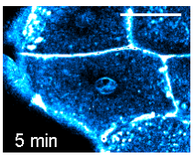

Movie M03: Nuclear envelope fragmentation revealed by THG signals

Time-lapse imaging focusing on THG signals at the level of the nuclear envelope. At 32-cell stage, end of the division at time 2min (indicated bottom left), maximum THG signal for the nuclear envelope at 10 min and disappearance at 11 min. Scale bar: 50µm. Raw data visualized with ImageJ software.

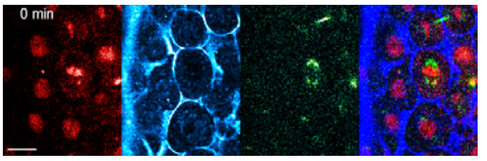

Movie M04: Mitosis steps revealed by 2PEF THG SHG microscopy

Time-lapse imaging at high magnification of a transgenic embryo *ßactin:H2B/mcherry* at 128-cell stage with 2PEF THG and SHG signals (see figure 2). Four panels are displayed with from left to right: red: 2PEF (H2B/mCherry fusion protein) image showing chromatin condensation, chromosome formation and displacements; blue: THG image; green: SHG image; three colors overlay. Scale bar: 20µm. Imaging time indicated top left. Raw data visualized with ImageJ software.

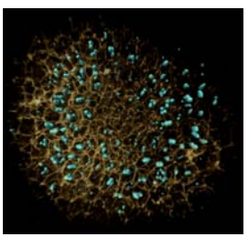

Movie M05: THG/SHG 4D imaging of the zebrafish embryo cleavage stages

THG/SHG 4D imaging of early zebrafish embryo, animal-pole view, 2D rendering of the whole imaged volume. Gold: THG signal revealing cell contours. Blue/Green: SHG signal revealing mitotic spindles (surface rendering). Raw data visualized with Amira software.

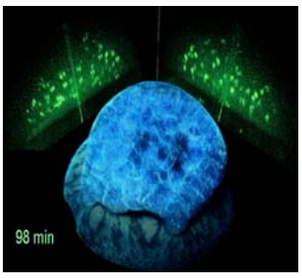

Movie M06: Conformal THG/SHG 4D imaging of the zebrafish embryo cleavage stages

Time-lapse imaging as described in Figure 2 from 2-cell stage to 1000-cell stage. In blue THG signal 3D rendering. In green: two different projections of SHG signal showing mitotic spindles in the entire blastoderm and yolk syncitium. Imaging time indicated bottom left. Raw data visualized with Amira software.

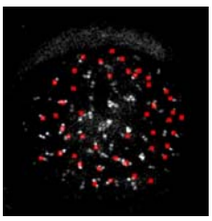

Movie M07: Algorithmic detection of mitotic spindles from SHG images

Greyscale image: XY projection of raw SHG images. Red overlay: detected SHG spots. Animal-pole view (see Figure 3). Augmented phenomenology with Amide software.

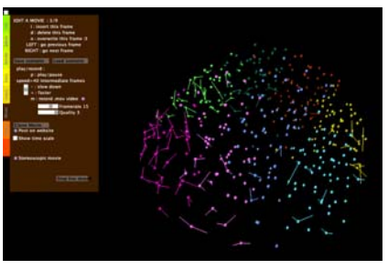

Movie M08: Interactive visualization of the digital embryo with the Mov-IT platform.

See figure S5.

Movie M09: Algorithmic segmentation of 32-cell stage blastomeres from THG images

Greyscale image: raw THG images. Color overlay: detected cells (see Figure 3). Visualization with Amide software.

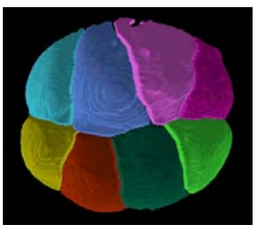

Movie M10: Digital embryo rendering of 8-cell stage blastomeres lineage

3D rendering of cell contours from THG image algorithmic segmentation. Animal-pole view. Each of the 8-cell stage blastomeres and its progeny displayed with a specific color (see figure3F-J). Mov-IT interactive visualization platform.

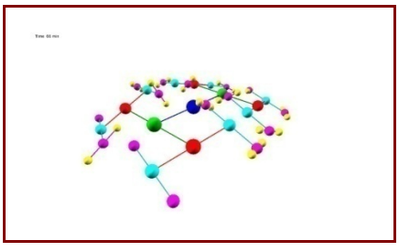

Movie M11: Spatial deployment of the cell lineage in a prototypical embryo

The prototype has been constructed from 6 different embryos from 2-cell stage to 256-cell stage (see figure 3). Visualized with Processing P5 software.

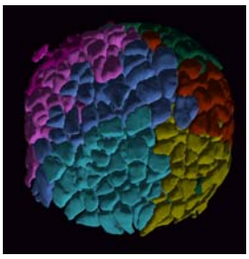

Movie M12: Digital embryo, division pseudo-wave pattern, and 8-cell stage blastomeres spatio-temporal lineage

Visualization of the division pseudo-waves with display of mother cell position (colored cube) and daughter cells' trajectories until next mitosis (plain lines) then 3D rendering of cell contours and coloring of 8-cell stage blastomeres lineage. Animal-pole view. Mov-IT interactive visualization platform.

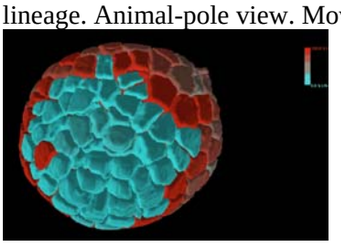

Movie M13. Digital embryo, division pseudo-wave pattern and cell cycle progression

Animal pole view from the 1-cell stage. Color code from blue to red indicates progression through the cell cycle in percentage of the cell cycle duration, red being the end. Mov-IT interactive visualization platform.

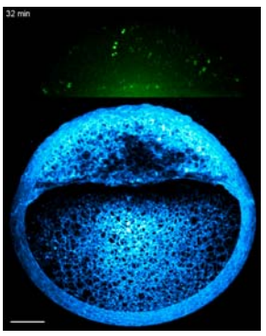

Movie M14: THG/SHG imaging during the last two divisions of yolk nuclei

Blue: THG. Green: SHG. Side-view of the whole embryo around 1000-cell stage. At minute 3-4 and minute 28-29 (indicated top right) divisions in the yolk start in the bilateral symmetry plane of the movie and progress on both sides giving rise to peripheral pseudo-waves. See Supplementary figure S13. Scale bar: 100µm. Raw data visualized with ImageJ software.

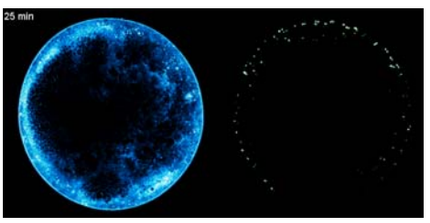

Movie M15. THG/SHG XY view of the yolk syncytial layer (YSL)

Section in the yolk cortical region. Blue: THG showing yolk structure. Green: SHG. See Supplementary figure S15. Raw data visualized with ImageJ software.

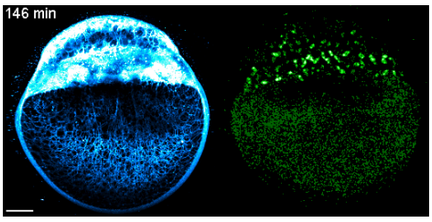

Movie M16: Artifact in the yolk syncitium formation as a consequence of physical constraint.

THG/SHG lateral view of an embryo constrained by agarose gel. Imaging time indicated top left. See Supplementary figure S17. Scale bar: 100µm. Raw data visualized with ImageJ software.